EUROPEAN ORGANISATION FOR PARTICLE PHYSICS

CERN-PPE/93-92
4 June 1993

Measurement of the Average b Hadron Lifetime in Z^0 Decays

The OPAL Collaboration

Abstract

A sample of 2610 electron candidates and 2762 muon candidates identified in hadronic Z^0 decays has been used to measure the average b hadron lifetime. These data were recorded with the OPAL detector during 1990 and 1991. Maximum likelihood fits to the distributions of the lepton impact parameters yield an average b hadron lifetime of

$$\tau_b = 1523 \pm 34 \pm 38 \ fs,$$

where the first error is statistical and the second systematic. This result is a weighted average over the semileptonic branching fractions and production rates of the b hadrons produced in Z^0 decays.

(Submitted to Z. Phys. C.)

The OPAL Collaboration

P.D. Acton[25], R. Akers[16], G. Alexander[23], J. Allison[16], K.J. Anderson[9], S. Arcelli[2], A. Astbury[28], D. Axen[29], G. Azuelos[18,a], J.T.M. Baines[16], A.H. Ball[17], J. Banks[16], R.J. Barlow[16], S. Barnett[16], R. Bartoldus[3], J.R. Batley[5], G. Beaudoin[18], A. Beck[23], G.A. Beck[13], J. Becker[10], C. Beeston[16], T. Behnke[27], K.W. Bell[20], G. Bella[23], P. Bentkowski[18], P. Berlich[10], S. Bethke[11], O. Biebel[3], I.J. Bloodworth[1], P. Bock[11], B. Boden[3], H.M. Bosch[11], M. Boutemeur[18], H. Breuker[8], P. Bright-Thomas[25], R.M. Brown[20], A. Buijs[8], H.J. Burckhart[8], C. Burgard[27], P. Capiluppi[2], R.K. Carnegie[6], A.A. Carter[13], J.R. Carter[5], C.Y. Chang[17], D.G. Charlton[8], S.L. Chu[4], P.E.L. Clarke[25], J.C. Clayton[1], I. Cohen[23], J.E. Conboy[15], M. Cooper[22], M. Coupland[14], M. Cuffiani[2], S. Dado[22], G.M. Dallavalle[2], S. De Jong[13], L.A. del Pozo[5], H. Deng[17], A. Dieckmann[11], M. Dittmar[4], M.S. Dixit[7], E. do Couto e Silva[12], J.E. Duboscq[8], E. Duchovni[26], G. Duckeck[11], I.P. Duerdoth[16], D.J.P. Dumas[6], P.A. Elcombe[5], P.G. Estabrooks[6], E. Etzion[23], H.G. Evans[9], F. Fabbri[2], B. Fabbro[21], M. Fierro[2], M. Fincke-Keeler[28], H.M. Fischer[3], D.G. Fong[17], M. Foucher[17], A. Gaidot[21], J.W. Gary[4], J. Gascon[18], N.I. Geddes[20], C. Geich-Gimbel[3], S.W. Gensler[9], F.X. Gentit[21], G. Giacomelli[2], R. Giacomelli[2], V. Gibson[5], W.R. Gibson[13], J.D. Gillies[20], J. Goldberg[22], D.M. Gingrich[30,a], M.J. Goodrick[5], W. Gorn[4], C. Grandi[2], F.C. Grant[5], J. Hagemann[27], G.G. Hanson[12], M. Hansroul[8], C.K. Hargrove[7], P.F. Harrison[13], J. Hart[8], P.M. Hattersley[1], M. Hauschild[8], C.M. Hawkes[8], E. Heflin[4], R.J. Hemingway[6], G. Herten[10], R.D. Heuer[8], J.C. Hill[5], S.J. Hillier[8], T. Hilse[10], D.A. Hinshaw[18], J.D. Hobbs[8], P.R. Hobson[25], D. Hochman[26], R.J. Homer[1], A.K. Honma[28,a], R.E. Hughes-Jones[8], R. Humbert[10], P. Igo-Kemenes[11], H. Ihssen[11], D.C. Imrie[25], A.C. Janissen[6], A. Jawahery[17], P.W. Jeffreys[20], H. Jeremie[18], M. Jimack[1], M. Jones[29], R.W.L. Jones[8], P. Jovanovic[1], C. Jui[4], D. Karlen[6], K. Kawagoe[24], T. Kawamoto[24], R.K. Keeler[28], R.G. Kellogg[17], B.W. Kennedy[15], S. Kluth[5], T. Kobayashi[24], D.S. Koetke[8], T.P. Kokott[3], S. Komamiya[24], L. Köpke[8], J.F. Kral[8], R. Kowalewski[6], J. von Krogh[11], J. Kroll[9], M. Kuwano[24], P. Kyberd[13], G.D. Lafferty[16], H. Lafoux[21], R. Lahmann[17], F. Lamarche[18], J.G. Layter[4], P. Leblanc[18], A.M. Lee[31], M.H. Lehto[15], D. Lellouch[26], C. Leroy[18], J. Letts[4], S. Levegrün[3], L. Levinson[26], S.L. Lloyd[13], F.K. Loebinger[16], J.M. Lorah[17], B. Lorazo[18], M.J. Losty[7], X.C. Lou[12], J. Ludwig[10], A. Luig[10], M. Mannelli[8], S. Marcellini[2], C. Markus[3], A.J. Martin[13], J.P. Martin[18], T. Mashimo[24], P. Mättig[3], U. Maur[3], J. McKenna[28], T.J. McMahon[1], J.R. McNutt[25], F. Meijers[8], D. Menszner[11], F.S. Merritt[9], H. Mes[7], A. Michelini[8], R.P. Middleton[20], G. Mikenberg[26], J. Mildenberger[6], D.J. Miller[15], R. Mir[12], W. Mohr[10], C. Moisan[18], A. Montanari[2], T. Mori[24], M. Morii[24], U. Müller[3], B. Nellen[3], H.H. Nguyen[9], S.W. O'Neale[1], F.G. Oakham[7], F. Odorici[2], H.O. Ogren[12], C.J. Oram[28,a], M.J. Oreglia[9], S. Orito[24], J.P. Pansart[21], B. Panzer-Steindel[8], P. Paschievici[26], G.N. Patrick[20], N. Paz-Jaoshvili[23], M.J. Pearce[1], P. Pfister[10], J.E. Pilcher[9], J. Pinfold[30], D. Pitman[28], D.E. Plane[8], P. Poffenberger[28], B. Poli[2], A. Pouladdej[6], T.W. Pritchard[13], H. Przysiezniak[18], G. Quast[27], M.W. Redmond[8], D.L. Rees[8], G.E. Richards[16], S.A. Robins[13], D. Robinson[8], A. Rollnik[3], J.M. Roney[28,b], E. Ros[8], S. Rossberg[10], A.M. Rossi[2], M. Rosvick[28], P. Routenburg[6], K. Runge[10], O. Runolfsson[8], D.R. Rust[12], M. Sasaki[24], C. Sbarra[2], A.D. Schaile[10], O. Schaile[10], W. Schappert[6], P. Scharff-Hansen[8], P. Schenk[4], B. Schmitt[3], H. von der Schmitt[11], M. Schröder[12], C. Schwick[27], J. Schwiening[3], W.G. Scott[20], M. Settles[12], T.G. Shears[5], B.C. Shen[4], C.H. Shepherd-Themistocleous[7], P. Sherwood[15], G.P. Siroli[2], A. Skillman[16], A. Skuja[17], A.M. Smith[8], T.J. Smith[28], G.A. Snow[17], R. Sobie[28,b], R.W. Springer[17], M. Sproston[20], A. Stahl[3], C. Stegmann[10], K. Stephens[16], J. Steuerer[28], R. Ströhmer[11], D. Strom[19], H. Takeda[24], T. Takeshita[24,c], S. Tarem[26], M. Tecchio[9], P. Teixeira-Dias[11], N. Tesch[3], M.A. Thomson[15].

E. Torrente-Lujan[22], S. Towers[28], G. Transtromer[25], N.J. Tresilian[16], T. Tsukamoto[24], M.F. Turner[8], D. Van den plas[18], R. Van Kooten[27], G.J. VanDalen[4], G. Vasseur[21], C.J. Virtue[7], A. Wagner[27], D.L. Wagner[9], C. Wahl[10], C.P. Ward[5], D.R. Ward[5], P.M. Watkins[1], A.T. Watson[1], N.K. Watson[8], M. Weber[11], P. Weber[6], P.S. Wells[8], N. Wermes[3], M.A. Whalley[1], B. Wilkens[10], G.W. Wilson[4], J.A. Wilson[1], V-H. Winterer[10], T. Wlodek[26], G. Wolf[26], S. Wotton[11], T.R. Wyatt[16], R. Yaari[26], A. Yeaman[13], G. Yekutieli[26], M. Yurko[18], W. Zeuner[8], G.T. Zorn[17].

[1]School of Physics and Space Research, University of Birmingham, Birmingham, B15 2TT, UK
[2]Dipartimento di Fisica dell' Università di Bologna and INFN, Bologna, 40126, Italy
[3]Physikalisches Institut, Universität Bonn, D-5300 Bonn 1, Germany
[4]Department of Physics, University of California, Riverside, CA 92521 USA
[5]Cavendish Laboratory, Cambridge, CB3 0HE, UK
[6]Carleton University, Dept of Physics, Colonel By Drive, Ottawa, Ontario K1S 5B6, Canada
[7]Centre for Research in Particle Physics, Carleton University, Ottawa, Ontario K1S 5B6, Canada
[8]CERN, European Organisation for Particle Physics, 1211 Geneva 23, Switzerland
[9]Enrico Fermi Institute and Dept of Physics, University of Chicago, Chicago Illinois 60637, USA
[10]Fakultät für Physik, Albert Ludwigs Universität, D-7800 Freiburg, Germany
[11]Physikalisches Institut, Universität Heidelberg, Heidelberg, Germany
[12]Indiana University, Dept of Physics, Swain Hall West 117, Bloomington, Indiana 47405, USA
[13]Queen Mary and Westfield College, University of London, London, E1 4NS, UK
[14]Birkbeck College, London, WC1E 7HV, UK
[15]University College London, London, WC1E 6BT, UK
[16]Department of Physics, Schuster Laboratory, The University, Manchester, M13 9PL, UK
[17]Department of Physics, University of Maryland, College Park, Maryland 20742, USA
[18]Laboratoire de Physique Nucléaire, Université de Montréal, Montréal, Quebec, H3C 3J7, Canada
[19]University of Oregon, Dept of Physics, Eugene, Oregon 97403, USA
[20]Rutherford Appleton Laboratory, Chilton, Didcot, Oxfordshire, OX11 0QX, UK
[21]DAPNIA/SPP, Saclay, F-91191 Gif-sur-Yvette, France
[22]Department of Physics, Technion-Israel Institute of Technology, Haifa 32000, Israel
[23]Department of Physics and Astronomy, Tel Aviv University, Tel Aviv 69978, Israel
[24]International Centre for Elementary Particle Physics and Dept of Physics, University of Tokyo, Tokyo 113, and Kobe University, Kobe 657, Japan
[25]Brunel University, Uxbridge, Middlesex, UB8 3PH UK
[26]Nuclear Physics Department, Weizmann Institute of Science, Rehovot, 76100, Israel
[27]Universität Hamburg/DESY, II Inst für Experimental Physik, 2000 Hamburg 52, Germany
[28]University of Victoria, Dept of Physics, P O Box 3055, Victoria BC V8W 3P6, Canada
[29]University of British Columbia, Dept of Physics, Vancouver BC V6T 1Z1, Canada
[30]University of Alberta, Dept of Physics, Edmonton AB T6G 2N5, Canada
[31]Duke University, Dept of Physics, Durham, North Carolina 27708-0305, USA

[a]Also at TRIUMF, Vancouver, Canada V6T 2A3
[b]And IPP, University of Victoria, Dept of Physics, P O Box 3055, Victoria BC V8W 3P6, Canada
[c]Also at Shinshu University, Matsumoto 390, Japan

1 Introduction

The lifetime of b hadrons was first measured at PEP [1, 2] and PETRA [3], then by the LEP collaborations [4, 5, 6, 7]. The average b hadron lifetime measurement has been used to calculate the Cabibbo-Kobayashi-Maskawa matrix element $|V_{cb}|$, one of the fundamental parameters of the Standard Model of Electroweak Interactions. At present theoretical uncertainties rather than experimental limitations dominate the calculation of $|V_{cb}|$. Recently, the first experimental measurements of the exclusive b hadron lifetimes have been made at PEP [2] and at LEP [7]. The lifetimes of individual b hadrons are expected to differ due to non-spectator effects by at most 10-20% and to be ordered in the sequence [8]

$$\tau\left(B^{-}\right) > \tau\left(\overline{B}_{s}^{0}\right) \geq \tau\left(\overline{B}_{d}^{0}\right) > \tau\left(\Lambda_{b}^{0}\right).$$

The average b hadron lifetime measurement is an important reference point to compare with these exclusive measurements and to test these theoretical predictions.

A measurement of the average b hadron lifetime using electron and muon candidates identified in hadronic Z^0 decays is presented in this paper following the technique used in Reference [4]. The data were collected with the OPAL detector during the 1990 and 1991 LEP runs, and represent an integrated luminosity of 20.6 pb^{-1}. The result presented here supersedes the result previously published by OPAL [4] which was based on the 1990 data sample alone. In addition to the increased statistics, several changes in the analysis have resulted in higher lepton identification efficiencies and higher purity b samples. Significant improvements in the treatment of the semileptonic decays of b and c hadrons have also been introduced.

2 The OPAL detector

The OPAL detector is described in detail elsewhere [9]. Only a brief overview of the components of OPAL that are relevant to this analysis is included here. The vertex chamber is a 1 m long cylindrical detector with inner and outer radii of 9 and 24 cm, respectively, surrounding an 8 cm radius, 1.3 mm thick carbon fiber beam pipe with a 0.1 mm aluminum inner lining. The volume of the chamber between radii of 9 and 17 cm is divided into 36 axial sectors with 12 wires each, and the remaining volume is divided into 36 stereo sectors with 6 wires each. The drift distance resolution is about 50 μm over most of the drift space, and increases to about 60 μm in the region near the anode plane corresponding to about 10% of the drift space. The vertex chamber measurements provide an impact parameter resolution of 40 μm on tracks in $Z^0 \rightarrow \mu^+\mu^-$ events. Surrounding the vertex chamber is a large volume jet chamber. The chamber has a 1.85 m outer radius, is 4 m long, and is divided into 24 azimuthal sectors, each sense wire plane consisting of 159 wires. Each of the wires provides three-dimensional coordinates calculated from the wire position, from a drift time measurement in the x-y plane and from a charge division measurement in the z direction.[1] The total charge on each wire is recorded for use in determining the mean ionization energy loss, $\mathrm{d}E/\mathrm{d}x$. The barrel region of the jet chamber is surrounded by a set of thin drift chambers, called

[1] The coordinate system is defined so that the z axis is in the direction of the electron beam, the x axis is horizontal and points approximately towards the center of the LEP ring, and the y axis is nearly vertical. The polar and azimuthal angles, θ and ϕ, are defined with respect to the z and x axes, respectively.

z chambers, that provide 6 precision measurements of the z coordinate. The vertex chamber and z chambers are mounted onto the support structure of the jet chamber and the whole assembly is positioned inside a pressure vessel, which is filled with an argon-methane-isobutane mixture at 4 bar. The pressure vessel is surrounded by a solenoidal coil that produces a uniform magnetic field of 0.435 T. The pressure vessel and the coil have a combined thickness of about two radiation lengths for particles at normal incidence. The components described above formed the central detector of OPAL for the 1990 run.

For the 1991 run a high-precision silicon microvertex detector surrounding a 5.3 cm-radius, 1.1 mm thick beryllium-composite beam pipe was inserted in OPAL. The old beam pipe was also replaced by an 8.0 cm radius carbon fiber pipe of 2.0 mm thickness. The analysis presented in this paper does not include information from the silicon detector because the precision of the impact parameter measurements from the wire vertex chamber are not an important limitation and because the silicon detector was only operational for about 2/3 of the 1991 data taking. It does, however, include the effects of the additional material in the inner detector in the 1991 run.

Positioned outside the coil is a barrel time-of-flight counter array consisting of 160 scintillator bars with phototube readout at both ends. A lead-glass electromagnetic calorimeter with a presampler, corresponding to 24.6 radiation lengths and about two hadronic interaction lengths, measures the positions and energies of showering particles. The magnet return yoke serves as a hadron calorimeter and is instrumented with 9 layers of streamer tubes. These detectors are surrounded by four layers of drift chambers for the detection of muons emerging from the hadron calorimeter. In the end cap region, electromagnetic and hadronic calorimeters provide energy measurements down to $|\cos\theta| = 0.98$, extending coverage to 98% of the full solid angle. Four layers of planar muon chambers, consisting of streamer tubes, track muons down to $|\cos\theta| = 0.985$ and extend the muon chamber coverage to 93% of the full solid angle.

At the time of this analysis the momentum resolution in the x-y plane for charged particles in the region $|\cos\theta| < 0.7$ was $(\sigma_p/p)^2_{xy} = 0.02^2 + (0.0015 \cdot p_{xy})^2$ [10], where p_{xy} is the momentum in the x-y plane in GeV/c. The resolution in $\mathrm{d}E/\mathrm{d}x$ for tracks having energy loss measurements on all 159 wires was 3.8%. The ratio of electromagnetic energy to track momentum for 10 GeV/c electrons had an r.m.s. width of about 8%. The resolution in the x-y plane of the distance of closest approach of the tracks to the beam spot, defined below, was less than 100 μm for all tracks which enter the lifetime fit. This value does not include the contribution from the spread of the average e^+e^- collision point.

The analysis presented here relies on the determination of the average intersection point of the LEP beams in the x-y plane. This average intersection point, or beam spot, was determined separately for each LEP fill and, statistics allowing, several times within a fill. The procedure for determining the beam spot [11] used tracks from both hadronic and leptonic decays of the Z^0, and resulted in an average precision of 15 μm and 10 μm in the x and y coordinates of the beam spot, respectively. The r.m.s. widths used for the beam intersection ellipsoid in this analysis were $157 \pm 20\,\mu m$ in x and $27 \pm 10\,\mu m$ in y. These values were determined using the 1990 data. The measured widths of the beam in the 1991 data are $147 \pm 4\,\mu m$ in x and $25 \pm 3\,\mu m$ in y. Unfolding the tracking resolution[2] yields beamspot widths of 146 μm in x and 17 μm in y. These are within the range of uncertainty quoted in this paper.

[2] These numbers were determined on data where silicon hits were present on tracks. The silicon impact parameter resolution is about 18 μm.

3 The event selection and simulated data sets

Hadronic events were selected using criteria described in Reference [12]. In addition, the central tracking chambers, the muon chambers, the barrel presampler, and the electromagnetic calorimeter were required to be fully operational. In each event, charged tracks and electromagnetic clusters with no association to a charged track were grouped into jets using the scaled invariant mass algorithm described in Reference [13]. Tracks used in the jet finding were required to pass within 5 cm of the beam spot in the x-y plane, and to have at least 20 hits in the jet chamber, a measured momentum component in the x-y plane above 0.15 GeV/c, and a total measured momentum below 65 GeV/c. Events were required to contain at least 7 charged tracks passing these cuts. A total of 320 995 (132 323) events in the 1991 (1990) sample were selected by these requirements.

Several Monte Carlo datasets were used in this analysis. Hadronic events were generated using the JETSET program tuned to OPAL data [14, 15]. Samples of 408 477 (195 998) JETSET events were passed through a detailed simulation [16] of the detector in the 1991 (1990) geometrical configuration. The data resulting from this simulation were reconstruction with the same algorithms as was used on OPAL data, and the processed data were then required to satisfy the event selection cuts described above. The fragmentation of b and c quarks was done using the Peterson scheme [17], with $\epsilon_b = 0.0035$ and $\epsilon_c = 0.06$.

Additional JETSET events were passed through a simplified simulation of the detector. In this simplified simulation, the number of hits assigned to each generated track was estimated, taking into account the 2-hit separation performance of each component of the central detector. The covariance matrix of the track parameters was then calculated, taking into account the estimated number of hits, their resolutions, and multiple Coulomb scattering. This covariance matrix was used to smear the track parameters about their generated values. The performance of the central detector was well described by the simplified simulation. The fragmentation of b and c quarks was done using the Peterson scheme, with the values of ϵ_b and ϵ_c quoted above. All Monte Carlo data referenced in this paper were processed using the detailed detector simulation unless stated otherwise.

The different detector configurations in the 1990 and 1991 runs produced negligible differences in this analysis and therefore the two sets of data were analyzed as a single data sample.

4 Modelling and branching ratios

The measurement of the average b hadron lifetime requires an understanding of heavy quark fragmentation, the momentum spectra of leptons from the semileptonic decays of b and c hadrons, and the corresponding semileptonic branching ratios. These issues are briefly discussed below; for a complete description see Reference [18].

The fragmentation functions for both b and c quarks have been measured at LEP, using charged leptons [19] and reconstructed D^* mesons [20]. The averages of these measurements, when interpreted in terms of the Peterson fragmentation function within the JETSET framework, give $\epsilon_b = 0.0055^{+0.0040}_{-0.0030}$ and $\epsilon_c = 0.05 \pm 0.02$. Expressed in terms of the mean fraction of the beam energy

Decay Mode	ISGW	ACCMM	ISGW**
$b \to \ell$	10.1	10.50±0.50	11.1
$b \to c \to \ell$	10.3	9.0±1.2	8.6
$b \to J/\psi \to \ell$		0.14±0.04	
$b \to \tau \to \ell$		0.5±0.2	
$c \to \ell$		9.6±0.9	

Table 1: Branching ratios, in percent, for the different b and c hadron decays for different semileptonic decay models. The ACCMM model is used to obtain the central result.

carried by the b or c hadron produced in the fragmentation process, $\langle x_E \rangle$, these measurements give $\langle x_E \rangle_b = 0.70 \pm 0.02$ and $\langle x_E \rangle_c = 0.51 \pm 0.02$. These parameters are used to obtain the average b hadron lifetime quoted in this paper, and the corresponding uncertainties are used in Section 10 to evaluate systematic errors. In practice, the Monte Carlo data were reweighted to correspond to a sample generated with the desired values of the Peterson fragmentation parameters. A reweighting technique was necessary because the simulation of a sufficient number of events would have required more computer resources than were available.

The CLEO Collaboration has used two models of semileptonic heavy flavour decay to fit their lepton momentum spectra [21], referred to as ACCMM and ISGW. The ACCMM model [22] is a free-quark model refined by the inclusion of QCD corrections. It has two input parameters, a Fermi momentum and the mass of the daughter quark produced in the heavy quark decay. The ISGW model [23] is based on a form-factor calculation of an explicit sum of momentum spectra calculated for individual three-body final states. No parameters were tuned by CLEO for this model. In addition to these two models, CLEO also fit their data using a modified version of the ISGW model, referred to as ISGW**. In fitting the ISGW** momentum spectrum to the CLEO data, the fraction of semileptonic $b \to \ell$ decays via the reaction $\overline{B} \to D^{**}\ell\nu$ was allowed to float freely, where D** represents a sum over the four excited D states with one unit of orbital angular momentum. For each model CLEO measures the branching ratios for $b \to \ell$ and $b \to c \to \ell$ decays. Reference [18] describes how these branching ratios are corrected for the presence of B_s mesons and b baryons in Z^0 decays (which are not present in CLEO data). The branching ratios applicable to OPAL data corresponding to each model are listed in Table 1. The average b hadron lifetime was obtained using the ACCMM model, and the ISGW model and its variant were used to evaluate systematic errors. The different models were simulated by reweighting from the momentum spectrum of the lepton in the rest-frame of the b or c hadron obtained from JETSET to the desired spectrum.

Finally, the branching ratios for the decays $b \to J/\psi \to \ell$, $b \to \tau \to \ell$, and $c \to \ell$ have changed significantly since the JETSET decay tables were last updated. Reference [18] discusses the latest values of these parameters, which are listed in Table 1. These branching ratios were also used in the determination of the average b hadron lifetime quoted in this paper.

5 The lepton selection

In addition to the requirements listed in Section 3, tracks considered as lepton candidates

satisfied the following conditions:

- The momentum, p, was at least 4.0 GeV/c.
- The transverse momentum with respect to the nearest jet axis, p_t, was at least 0.8 GeV/c for electron candidates and 1.0 GeV/c for muon candidates. The p_t was determined with the candidate track included in the jet axis calculation.
- The absolute value of the cosine of the polar angle was less than 0.7.
- At least 80 hits in the jet chamber were associated with the track.
- At least 3 hits in the z chambers were associated with the track.
- At least 6 hits in an axial sector of the vertex chamber were associated with the track.
- Less than half of the axial vertex chamber hits were registered on the ionization tail of earlier hits. This criterion was applied because the drift distance resolution of these hits was worse by a factor of two compared to the resolution of the first hits registered on the wires. Approximately 22% of the lepton candidates were rejected by this cut after all other cuts were applied.

Tracks satisfying these criteria were subjected to the following lepton identification procedures [18].

Electron candidates were required to be consistent with the expected signature for electrons in their measured $\mathrm{d}E/\mathrm{d}x$, in the pulse height registered in the electromagnetic presampler, and in the lateral spread of the associated electromagnetic shower. In addition, the measured electromagnetic energy divided by the reconstructed track momentum, E/p, had to lie between 0.7 and 1.4. Candidate photon conversion electrons were tagged [18] and removed from the sample. The background in the electron candidate sample came principally from misidentified hadron tracks, photon conversions which failed the tagging algorithm, and the Dalitz decay of neutral mesons. Unless stated otherwise the term "background" does not include leptons from the semileptonic decay of c hadrons produced in $Z^0 \to c\bar{c}$ decays. The efficiencies and hadronic background fraction were obtained from the data following the method described in Reference [18]. There were 2610 electron candidates identified in the data sample.

Muon candidates were selected from the subset of central detector tracks associated with track segments in the muon chambers. In addition, the $\mathrm{d}E/\mathrm{d}x$ measured in the jet chamber was required to be consistent with the expected value for muons in order to reduce the background from long-lived charged kaon decays to muons. The identification efficiency was determined from the Monte Carlo simulation and is nearly independent of both p and p_t. The background in the muon candidate sample was also determined from the Monte Carlo simulation and is due to decays in flight of charged pions and kaons, and hadrons that either passed through the calorimeters without interacting strongly or showered in such a way that one or more particles reached the muon chambers to fake a muon signal. The probability that a hadron was misidentified as a muon did not depend strongly on the kinematic variables. The efficiency was cross-checked using data samples of $Z^0 \to \mu^+\mu^-$ decays and $e^+e^- \to e^+e^-\mu^+\mu^-$ events, and the background estimate was cross-checked using data samples of $\mathrm{K}^0_s \to \pi^+\pi^-$ decays and τ decays to three charged pions. These comparisons formed the basis for estimating the systematic uncertainties in the muon identification. There were 2762 muon candidates identified in the data sample.

6 The lifetime fit

The average b hadron lifetime is determined from maximum likelihood fits to the impact parameter distributions of the two lepton samples. In this analysis, the term impact parameter refers to the smallest distance in the x-y plane between the track in question and the beam spot. The sign of the impact parameter is positive if the angle in the x-y plane between the vector from the beam spot to the point of closest approach of the track and the axis of the jet containing the lepton candidate is less than 90°, otherwise it is negative.

The lifetime measurement method used here is the same as that previously used by OPAL [4]. The observed impact parameter distribution is determined by particle lifetimes and decay kinematics, and by the detector resolution. In this analysis, the impact parameter distribution is described in terms of a convolution of the distributions expected from the underlying physics processes with a resolution function determined from the data. The impact parameter distributions are divided into five components for which separate probability density functions are constructed. They are

1. Leptons arising from the semileptonic decay of b hadrons. These are referred to as primary b decays.
2. Leptons arising from the semileptonic decay of c hadrons or from the decay of τ leptons which themselves arise from b hadron decay. These are referred to as cascade decays.
3. Leptons arising from the semileptonic decay of c hadrons that do not come from b hadron decay. These are referred to as primary c decays.
4. Hadrons that are misidentified as leptons.
5. Decays in flight of charged pions and kaons to muons, photon conversions and Dalitz decays of neutral mesons.

The first and second components are functions of the average B hadron lifetime, τ_b, whereas the other components have little or no dependence on τ_b.

The compositions of the lepton samples are given in Table 2. The Monte Carlo electrons were selected using all electron identification criteria and were then weighted by the ratio of the electron identification efficiencies (as a function of p and p_t) obtained from the Monte Carlo to the efficiencies measured from the data. Unless stated otherwise this procedure is always applied to the Monte Carlo electrons. The muon identification efficiencies are well reproduced in the Monte Carlo [18] and therefore no correction was required. The electron sample hadronic background fraction, measured from the data, was used in the calculation of the sample fractions. The Monte Carlo gives a reliable prediction for the probability of identifying a hadron as a muon [18], so the expected number of background tracks in the muon sample was used in the calculation of the muon sample fractions. Figure 1 shows the momentum and transverse momentum distributions of the lepton samples. There is good agreement between the predicted and observed shapes of these distributions.

The likelihood function to be maximized is

$$\mathcal{L} = \prod_{j=1}^{N} \left[f_1 P_1(\tau_b, d_0^j, \sigma^j) + f_2 P_2(\tau_b, d_0^j, \sigma^j) + f_3 P_3(d_0^j, \sigma^j) + f_4 P_4(d_0^j, \sigma^j) + f_5 P_5(d_0^j, \sigma^j) \right], \qquad (1)$$

electron sample components		% of total
1.	$b \rightarrow e$	78.5
2.	$b \rightarrow (c \text{ or } \tau) \rightarrow e$	10.9
3.	$c \rightarrow e$	6.8
4.	hadrons misidentified as electrons	3.5
5.	photon conversions and Dalitz decays	0.3
muon sample components		% of total
1.	$b \rightarrow \mu$	75.5
2.	$b \rightarrow (c \text{ or } \tau) \rightarrow \mu$	10.0
3.	$c \rightarrow \mu$	5.7
4.	hadrons misidentified as muons	7.0
5.	decay in flight of charged pions and kaons	1.8

Table 2: The composition of the lepton samples.

where d_0^j is the measured impact parameter of the lepton candidate j, σ^j is the assigned uncertainty in d_0^j as described in Section 8, P_i is the probability density function for component i, whose determination is described in the following section, f_i is the fraction of the lepton sample due to component i, as given in Table 2, and N is the total number of lepton candidates. The only free parameter in the fit is τ_b.

7 Determination of the probability density functions

The probability density functions for components 1, 2, and 3 were constructed by convoluting the underlying physics distributions with the resolution function described in the next section. The underlying physics distributions are the impact parameter distributions that would be obtained from a detector with perfect impact parameter resolution. This convolution was performed track-by-track since the resolution depends on, amongst other variables, the track momentum and the track direction.

The underlying physics distributions for components 1 to 3 were determined using a sample of 6.43 million $Z^0 \rightarrow b\bar{b}$ and 1.02 million $Z^0 \rightarrow c\bar{c}$ events generated with JETSET. These events were processed using the simplified simulation of the OPAL detector. The impact parameters were taken directly from the generated information before the detector simulation, but only particles whose reconstructed tracks passed the track quality and kinematic cuts were entered into these distributions. The lepton identification cuts were not applied in this case because the simplified Monte Carlo gives a poor description of the identification variables. Instead, the leptons were weighted using tables of lepton identification efficiencies as a function of p and p_t. The muon table was obtained from the full Monte Carlo and the electron table was obtained directly from the data [18]. The impact parameters were calculated relative to the event-by-event production point instead of the average beam spot, and their signs were determined using the jet axes reconstructed from the charged tracks and unassociated electromagnetic clusters obtained after the detector simulation. This procedure was necessary because the signing of the impact parameters is determined by the

other particles in the jet whereas the resolution function applies only to the lepton candidate track, and therefore cannot account for signing mistakes due to imprecise estimates of the b hadron direction. These distributions were parametrized using a sum of exponential functions in order to facilitate an analytic convolution with the resolution function. The distributions were expressed in terms of the impact parameter divided by the product of the speed of light and the average generated lifetime of the sample in question. For component 1 this is the generated b hadron lifetime, for component 2 this is the sum of the generated b hadron lifetime and the average generated lifetime of c hadrons, and for component 3 this is the average generated lifetime of c hadrons. The generated lifetime for b hadrons was 1500 fs, and the average generated lifetime for c hadrons was 670 fs for component 2, the cascade decays, and 717 fs for component 3, the primary charm decays. The average generated lifetimes for c hadrons are different for components 2 and 3 because the mixture of c hadrons in each sample is different. The underlying physics distribution for electrons from b decays is shown in Figure 2 with the result of the fit.

The probability density functions for component 4, the misidentified hadrons, were determined directly from the data. The impact parameter distribution of the electron hadronic background was obtained from the set of tracks that passed all electron selection criteria, except the ratio E/p was required to be in the range 0.2 to 0.6 and the electromagnetic presampler pulse height cut was not applied. Monte Carlo studies indicated that the resulting sample is completely dominated by hadron tracks. This distribution was then normalized and fitted with a Gaussian and exponential tails to yield an analytic probability density function. Similarly for the muon hadronic background, the corresponding probability density function was derived from the set of tracks that passed all track quality and kinematic cuts but failed both the electron and muon identification criteria. The resulting sample was also dominated by hadrons.

The probability density function for component 5 of the electron sample was chosen to be identical to the electron misidentification probability density function. The broadening of the impact parameter distribution due to extrapolating tracks from converted photons back to the origin was less than the width resulting from the tracking resolution and the width of the beam spot because of the high momentum cut and the axial vertex chamber hit requirement. This consideration, coupled with the small fraction (0.3%) of the data ascribed to this component, justify the use of the misidentification distribution. The probability density function for component 5 of the muon sample was determined from a large sample of pion and kaon decays in hadronic events simulated by the Monte Carlo.

8 Determination of the resolution function

The impact parameter resolution depends on the variables used to select the lepton candidates. Therefore the detector resolution function was measured with the set of tracks that passed all track quality and kinematic cuts but failed the lepton identification. In addition, tracks were selectively discarded to bring the distributions of p, p_t, the number of jet chamber hits, and the number of vertex chamber hits into agreement with the distributions observed from the lepton samples for these quantities. Since the resolution function is applied to leptons from bottom and charm decays, the p and p_t distributions for components 4 and 5 (obtained from the Monte Carlo) were subtracted from the corresponding distributions for the lepton samples before selectively discarding tracks. The distributions of the number of jet chamber hits and vertex chamber hits show no significant

difference between the prompt lepton sources and components 4 and 5. The tracks remaining after this "trimming" procedure are called resolution function tracks. The resolution functions for electrons and muons may differ due to the different p_t cuts, the different lepton identification cuts, and the differences in the shapes of the distributions of p, p_t, and the number of jet chamber and vertex chamber hits.

The distribution of the impact parameters divided by their calculated uncertainties for resolution function tracks from the data is shown in Figure 3a. The uncertainties were calculated according to the formula

$$\sigma^2 = a^2 \cdot V_{dd} + \sin^2\phi \cdot S_x^2 + \cos^2\phi \cdot S_y^2, \tag{2}$$

where V_{dd} is the variance of the impact parameter from the track fit, which includes contributions due to multiple Coulomb scattering, S_x and S_y are the widths of the beam spot in x and in y, respectively, ϕ is the azimuthal angle of the track momentum vector measured at the point of closest approach of the track to the beam spot, and a is a parameter which would be unity if the estimate of the impact parameter variance was consistent with the true reconstructed errors. In practice the true deviations of the measured impact parameters are not perfectly described by V_{dd}. Although σ describes the measurement accuracy on most tracks, there is a second, broader component to the distribution that comes from pattern recognition mistakes, large angle multiple scattering, imperfect detector calibrations, and the presence of long-lived particles in the data sample. Consequently, the resolution function was parametrized as the sum of two Gaussians,

$$R(d_0, V_{dd}) = \frac{(1-f)}{\sqrt{2\pi}\sigma} \exp\left(-\frac{d_0^2}{2\sigma^2}\right) + \frac{f}{\sqrt{2\pi}\sigma_t} \exp\left(-\frac{d_0^2}{2\sigma_t^2}\right), \tag{3}$$

where f is the fractional area of the broad component of the distribution and

$$\sigma_t^2 = w^2 \cdot a^2 \cdot V_{dd} + \sin^2\phi \cdot S_x^2 + \cos^2\phi \cdot S_y^2 \tag{4}$$

is the square of the width of the broad component. The parameters a, f, and w were determined from a maximum likelihood fit to the resolution function tracks. The width of the narrower Gaussian (in d_0/σ) was constrained to unity in the fit. Only the entries with a negative impact parameter were used in the fit, since tracks from the decays of long-lived particles introduce an asymmetry in the distribution, as seen in Figure 3a. Monte Carlo studies indicated that the resolution function track sample had an excess of entries in the region $d_0/\sigma < -15$ compared to the Monte Carlo leptons, so the fit was also limited to the region $d_0/\sigma > -15$. A different choice for this lower bound will be discussed in Section 10. The fitted values of the parameters describing the resolution function appear in Table 3 under the column labelled "raw."

The resolution function obtained from the data must be corrected for tracks produced in the decays of long-lived hadrons that are assigned a negative impact parameter, and for any bias introduced by using hadrons to determine the resolution properties of leptons. The correction was determined from the Monte Carlo as follows. Shown in Figure 3b is the distribution of resolution function tracks from the Monte Carlo dataset obtained using the same criteria as applied to the data. Figure 3c shows the distribution for the Monte Carlo electrons after subtracting the contribution to the impact parameters due to the lifetime of the parent hadron. This was done by calculating the true impact parameters of the tracks relative to the Z^0 decay point, using only the generated information, and subtracting these from the measured impact parameters of the tracks after the detector simulation. Therefore the difference between the measured and true impact parameters

parameter	electrons		muons	
	raw	corrected	raw	corrected
a	1.053 ± 0.025	1.049 ± 0.040	1.084 ± 0.025	1.034 ± 0.038
f	0.0679 ± 0.0052	0.0438 ± 0.0073	0.0651 ± 0.0047	0.0389 ± 0.0065
w	7.20 ± 0.30	4.92 ± 0.55	7.54 ± 0.29	5.42 ± 0.65
S_x	$157 \pm 20\,\mu m$			
S_y	$27 \pm 10\,\mu m$			

Table 3: The parameters describing the resolution functions. The errors are statistical only.

contains only contributions from the detector resolution and from the width of the beam spot in the x-y plane. The Monte Carlo electron distribution was fit with a double Gaussian in the region $|d_0/\sigma| < 15$ to extract the resolution function parameters. The a and w parameters from the data were scaled by the ratios of these quantities obtained from the Monte Carlo lepton fits and the Monte Carlo hadron fits. The f parameter from the data was corrected by subtracting the f obtained from the Monte Carlo hadron fit and adding the f obtained from the Monte Carlo lepton fit. This was necessary because the Monte Carlo does not account for most of the entries in the tails caused by the degraded resolution near the vertex chamber anode planes. The corrected resolution function parameters for the data are given in Table 3 and define the resolution function used in the likelihood fits for the lifetime.

9 Results and Consistency Checks

The results of the one parameter fits to the impact parameter distributions are given in Table 4. The curves in Figure 4 display the results of the fits. The χ^2 were calculated from the binned data shown in Figure 4.

	electrons	muons
N_{cand}	2610	2762
τ_b (fs)	1528±48	1519±49
$\chi^2/d.f.$	33.6/37	31.2/37

Table 4: The results of fits to the OPAL data. The errors are statistical only.

Several checks were performed to look for possible detector-related systematic effects. In various tests, the lepton samples were split into positive and negative tracks, into horizontal and vertical quadrants, and into high and low ranges of p and p_t. The data were also divided according to the distance of the tracks from the vertex chamber anode planes, and according to the year they were recorded. The sensitivity of the result to tracks with large impact parameters was investigated by performing the likelihood fit over a reduced range. Finally, the data were divided into 2 bins

	electrons	muons
N_{cand}	4541	4150
τ_b (fs)	1280±31	1288±33
$\chi^2/d.f.$	41.4/37	42.9/37

Table 5: The results of fits to the Monte Carlo lepton samples. The weighted mean of the two results is $1284 \pm 23\ fs$. The generated lifetime in these samples was $1300\ fs$.

according to the $|\cos\theta|$ of the axis of the jet which contains the lepton candidate. The results from the subsamples were consistent in each case.

The method outlined above was also applied to the Monte Carlo data which was generated with a b hadron lifetime of $1300\ fs$. This sample was statistically independent from the ones used to determine the underlying physics distributions for components 1 to 3. Separate resolution functions were determined for this Monte Carlo sample using the procedure described above. The probability density functions for components 4 and 5 were similarly determined from this Monte Carlo sample. The fitted lifetimes are given in Table 5. The results of each individual fit and the average of the two fits are in good agreement with the generated lifetime.

source	error on τ_b (fs)
BR($b \to \ell$)	3
BR($b \to c \to \ell$)	3
BR($c \to \ell$)	8
vector versus scalar c meson production in b decays	1
BR($b \to J/\psi \to \ell$)	1
BR($b \to \tau \to \ell$)	1
vector versus scalar c meson production in $Z^0 \to c\bar{c}$ events	1
D_s production in $Z^0 \to c\bar{c}$ events	3
Λ_c production in $Z^0 \to c\bar{c}$ events	4
b quark fragmentation	17
c quark fragmentation	7
b decay models	10
c decay models	9
b hadron lifetime in the Monte Carlo	4
B^+ meson lifetime and branching fraction in the Monte Carlo	8
jet invariant mass cutoff	8
beam spot size and position	10
resolution function statistics and parametrization	15
total common systematic error	33

Table 6: Summary of systematic errors common to the electron and muon samples.

10 Determination of systematic errors

The systematic errors fall into two categories: errors common to both the electron and the muon samples, and errors that are uncorrelated between the two samples. Table 6 lists the common systematic errors. They were determined as follows:

- The semileptonic branching fraction of b hadrons was varied by $\pm 5\%$.
- The branching fraction of cascade decays was varied by $\pm 13\%$.
- The branching fraction of primary c decays was varied by $\pm 10\%$.
- The ratio of vector to scalar c mesons produced in b decays was varied from 2.5 to 4.0. This changed the average c hadron lifetime and average semileptonic branching fraction of c hadrons in this sample by $\pm 1\%$.
- The branching fraction of b$\rightarrow J/\psi \rightarrow \ell$ decays was varied by $\pm 30\%$.
- The branching fraction of b$\rightarrow \tau \rightarrow \ell$ decays was varied by $\pm 40\%$.
- The ratio of vector to scalar c mesons produced in $Z^0 \rightarrow c\bar{c}$ decays was varied from 2.5 to 4.0. This changed the average c hadron lifetime and average semileptonic branching fraction of c hadrons in this sample by $\pm 1\%$.
- The fraction of D_s mesons produced in $Z^0 \rightarrow c\bar{c}$ decays was varied from 10 to 20%.
- The fraction of Λ_c baryons produced in $Z^0 \rightarrow c\bar{c}$ decays was varied from 5 to 15%.
- The fragmentation parameter ϵ_b in the Peterson scheme was varied between 0.0025 and 0.0095, corresponding to $\langle x_E \rangle_b = 0.72$ and $\langle x_E \rangle_b = 0.68$. The measured lifetime decreases as the $\langle x_E \rangle$ increases.
- The fragmentation parameter ϵ_c in the Peterson scheme was varied between 0.030 and 0.070, corresponding to $\langle x_E \rangle_c = 0.53$ and $\langle x_E \rangle_c = 0.49$. The measured lifetime increases as the $\langle x_E \rangle$ increases.
- The ISGW model and its variant, ISGW**, were used to simulate the semileptonic b decays and cascade decays. The b hadron lifetime was evaluated in each case, and the maximum deviation from the result obtained using the ACCMM model was taken as a systematic error. The ISGW variant, ISGW**, has the softest momentum spectrum in the rest frame of the parent hadron and resulted in the highest measured lifetime.
- The ISGW model was used to simulate the primary c decays. The deviation of the resulting b hadron lifetime from the result obtained using the ACCMM model was taken as a systematic error. The ACCMM model has the harder rest frame momentum spectrum and gives the higher measured lifetime.
- The b hadron lifetime in the Monte Carlo used to determine the correction factors for the resolution function was varied by $\pm 15\%$.

- The lifetime and semileptonic branching fraction of the B^+ meson were increased by 20%, keeping the properties of all other b hadrons fixed. This tests the validity of the statement that the fitted lifetime corresponds to an average weighted by production rates and semileptonic branching ratios.

- The data were processed with the jet finding parameter x_{min} set to 64 $(GeV/c^2)^2$ instead of 49 $(GeV/c^2)^2$, without changing the Monte Carlo. This increases the maximum invariant mass allowed for any single jet, and results in a 5% decrease in the average number of jets per event. This accounts for possible biases introduced in the jet finding by the imperfect Monte Carlo simulation of the detector response.

- The assumed size and position of the beam spot were varied by their estimated uncertainties.

- Each parameter describing the corrected resolution function was varied within its statistical accuracy, producing a maximum variation in τ_b of 8 fs. If the resolution function tracks are not selectively discarded before they are used in the resolution function fits then the lifetime shifts by 10 fs. This is taken as a systematic error to account for biases in the resolution function correction procedure. The region over which the resolution function fits were performed was changed from $|d_0/\sigma| < 10$ to $|d_0/\sigma| < 20$ and resulted in an average lifetime shift of 7 fs. These three effects are added in quadrature to yield the total resolution function systematic error of 15 fs.

The total systematic error common to the electron and muon samples was ± 33 fs, determined by adding the individual contributions in quadrature. The effects of the uncertainty due to the Λ_b polarization on the determination of the average lifetime were estimated to be negligible.

source	error on τ_b (fs)	
	electrons	muons
background to the lepton samples	3	10
electron identification relative efficiencies	20	–
electron bremsstrahlung	10	–
$b \to \ell$ physics distribution statistics	19	20
$b \to c \to \ell$ physics distribution statistics	9	8
$c \to \ell$ physics distribution statistics	6	2
misidentification function statistics	6	2
$K \to \mu$ and $\pi \to \mu$ decays	–	4
total	32	24

Table 7: Summary of systematic errors specific to each of the two lepton samples.

The systematic errors specific to one lepton species or the other are given in Table 7. They were determined as follows:

- The electron and muon background normalizations were allowed to vary by $\pm 10\%$ and $\pm 13\%$ [18], respectively.

- Electrons from primary b decays, cascade decays and primary c decays have different isolation properties, and as a result the electron identification efficiency is expected to differ for each source. According to the Monte Carlo simulation, the efficiency for electrons from primary c decays differs from the efficiency for electrons from primary b decays by 40%, and the efficiency for electrons from cascade decays differs from that of electrons from primary b decays by 15%. The effect of nearby particles on the identification efficiency is known to be overestimated in the Monte Carlo simulation. The track quality requirements used in this analysis favor isolated tracks, which results in a reduced sensitivity to the isolation properties of the electron identification requirements compared to that of Reference [24]. This allows the use of the Monte Carlo prediction as the central value and the full size of the predicted differences is used in assessing the systematic error.

- The underlying physics distributions for the electrons were corrected for the effects of electron bremsstrahlung. The corresponding change in the lifetime was taken as a systematic error.

- Each parameter of the functions describing the $b \rightarrow \ell$ underlying physics distributions was varied by its statistical uncertainty. The maximum variation in the lifetime was taken as a systematic error.

- Each parameter of the functions describing the $b \rightarrow c \rightarrow \ell$ underlying physics distributions was varied by its statistical uncertainty. The maximum variation in the lifetime was taken as a systematic error.

- Each parameter of the functions describing the $c \rightarrow \ell$ underlying physics distributions was varied by its statistical uncertainty. The maximum variation in the lifetime was taken as a systematic error.

- Each parameter of the functions describing the misidentification probability density functions was varied by its statistical uncertainty. The maximum variation in the lifetime was taken as a systematic error.

- Each parameter of the probability density function describing the charged pion and kaon decays to muons was varied by its statistical uncertainty. The maximum variation in the lifetime was taken as a systematic error.

Adding each contribution in quadrature results in the total uncorrelated systematic errors listed in Table 7.

The results from the electron and muon fits are combined, weighting them by their statistical errors and the systematic errors that were not correlated between the two samples. The result is

$$\tau_b = 1523 \pm 34 \pm 38 \ fs,$$

where the first error is statistical and the second systematic.

11 Conclusion

The average b hadron lifetime has been measured using the impact parameters of electron and muon candidates identified in the 1990 and 1991 OPAL data samples. The result is $\tau_b = 1523 \pm 34 \pm 38\ fs$. This value is a weighted average over the production fractions and semileptonic branching ratios of the b hadrons produced in hadronic Z^0 decays, and supersedes the result previously published by OPAL [4]. The major physics limitations in the precision of this result come from our current understanding of heavy quark fragmentation and the details of the semileptonic decays of heavy quarks.

The average b hadron lifetime is used to calculate the Cabibbo-Kobayashi-Maskawa matrix element $|V_{cb}|$. Following the procedure of Reference [5] and using the result of this paper, one finds $|V_{cb}| = 0.0399 \pm 0.0007 \pm 0.0031$ within the framework of the ACCMM model. The first error is due to the combined statistical and systematic uncertainty in τ_b and the second error is dominated by the uncertainties in the ACCMM model. Using a different model of semileptonic heavy quark decay will give a significantly different result for $|V_{cb}|$. Further progress in understanding b hadron decays is needed to take full advantage of the improved precision of the average b hadron lifetime measurement.

Acknowledgements

It is a pleasure to thank the SL Division for the efficient operation of the LEP accelerator, the precise information on the absolute energy, and their continuing close cooperation with our experimental group. In addition to the support staff at our own institutions we are pleased to acknowledge the
Department of Energy, USA,
National Science Foundation, USA,
Texas National Research Laboratory Commission, USA,
Science and Engineering Research Council, UK,
Natural Sciences and Engineering Research Council, Canada,
Fussefeld Foundation,
Israeli Ministry of Energy and Ministry of Science,
Minerva Gesellschaft,
Japanese Ministry of Education, Science and Culture (the Monbusho) and a grant under the Monbusho International Science Research Program,
German Israeli Bi-national Science Foundation (GIF),
Direction des Sciences de la Matière du Commissariat à l'Energie Atomique, France,
Bundesministerium für Forschung und Technologie, Germany,
National Research Council of Canada,
A.P. Sloan Foundation and Junta Nacional de Investigação Científica e Tecnológica, Portugal.

References

[1] MARK-II Collab., A. Lockyer et al., Phys. Rev. Lett. **51** (1983) 1316;
MARK-II Collab., R. A. Ong et al., Phys. Rev. Lett. **62** (1989) 1236;
MAC Collab., W. Ash et al., Phys. Rev. Lett. **58** (1987) 640;
HRS Collab., J. M. Brom et al., Phys. Lett. **B195** (1987) 301;
DELCO Collab., D. E. Klem et al., Phys. Rev. **D37** (1988) 41.

[2] Mark II Collab., S. R. Wagner et al., Phys. Rev. Lett. **64** (1990) 1095.

[3] TASSO Collab., W. Braunschweig et al., Z. Phys. **C44** (1989) 1;
JADE Collab., J. Hagemann et al., Z. Phys. **C48** (1990) 401.

[4] OPAL Collab., Phys. Lett. **B274** (1992) 513.

[5] L3 Collab., B. Adeva et al., Phys. Lett. **B270** (1991) 111.

[6] ALEPH Collab., D. Decamp et al., Phys. Lett. **B257** (1991) 492;
ALEPH Collab., D. Decamp et al., Phys. Lett. **B295** (1992) 174;
DELPHI Collab., P. Abreu et al., Zeit. Phys. **C53** (1992) 567.

[7] ALEPH Collab., D. Buskulic et al., Phys. Lett. **B295** (1992) 396;
ALEPH Collab., D. Buskulic et al., Phys. Lett. **B297** (1992) 449;
ALEPH Collab., D. Buskulic et al., *Measurement of the* $\overline{B}^0$ *and* B^- *Meson Lifetimes*, CERN-PPE/93-42, submitted to Phys. Lett. B;
DELPHI Collab., P. Abreu et al., *Measurement of* Λ_b *Production and Lifetime in* Z^0 *Hadronic Decays*, CERN-PPE/93-32, submitted to Phys. Lett. B;
DELPHI Collab., P. Abreu et al., Z. Phys. **C57** (1993) 181;
OPAL Collab., G. Alexander et al., Phys. Lett. **B266** (1991) 485;
OPAL Collab., P. Acton et al., *Measurement of the* B^0 *and* B^+ *Lifetimes*, CERN-PPE/93-33, submitted to Phys. Lett. B.

[8] I. I. Bigi, N. G. Uraltsev, Phys. Lett. **B280** (1992) 271;
G. Altarelli, S. Petrarca, Phys. Lett. **B261** (1991) 303.

[9] OPAL Collab., K. Ahmet et al., Nucl. Inst. and Meth. **A305** (1991) 275.

[10] O. Biebel et al., Nucl. Inst. and Meth. **A323** (1992) 169.

[11] OPAL Collab., P. D. Acton et al., Phys. Lett. **B273** (1991) 355.

[12] OPAL Collab., G. Alexander et al., Z. Phys. **C52** (1991) 175.

[13] OPAL Collab., M. Z. Akrawy et al., Phys. Lett. **B235** (1990) 389. The E0 recombination scheme was used in the jet finding with the invariant mass-squared cut-off x_{min} set to $(7\,GeV/c^2)^2$.

[14] T. Sjöstrand, Comp. Phys. Comm. **39** (1986) 347;
T. Sjöstrand, M. Bengtsson, Comp. Phys. Comm. **43** (1987) 367.

[15] OPAL Collab., M. Z. Akrawy et al., Z. Phys. **C47** (1990) 505.

[16] J. Allison et al., Nucl. Instr. and Meth. **A317** (1992) 47.
J. Allison et al., Comp. Phys. Comm. **47** (1987) 55;
R. Brun et al., GEANT 3, Report DD/EE/84-1, CERN (1989).

[17] C. Peterson et al., Phys. Rev. **D27** (1983) 105.

[18] OPAL Collab., P. Acton et al., *Measurement of* $\Gamma\left(Z^0 \to b\bar{b}\right)/\Gamma\left(Z^0 \to hadrons\right)$ *using Leptons*, CERN-PPE/93-46, to appear in Z. Phys. C.

[19] ALEPH Collab., D. Decamp et al., Phys. Lett. **B244** (1990) 623;
DELPHI Collab., P. Abreu et al., Z. Phys. **C56** (1992) 47;
L3 Collab., B. Adeva et al., Phys. Lett. **B288** (1992) 412;
OPAL Collab., M. Z. Akrawy et al., Phys. Lett. **B263** (1991) 311.

[20] ALEPH Collab., D. Decamp et al., Phys. Lett. **B266** (1991) 218;
OPAL Collab., G. Alexander et al., Phys. Lett. **B262** (1991) 341.

[21] CLEO Collab., S. Henderson et al., Phys. Rev. **D45** (1992) 2212;
M. Worris, Ph.D. Thesis, *Measurements of the B meson Semileptonic Branching Fraction*, August 1991, CLNS 91-05.

[22] G. Altarelli et al., Nucl. Phys. **B208** (1982) 365.

[23] N. Isgur et al., Phys. Rev. **D39** (1989) 799.

[24] OPAL Collab., P. D. Acton et al., *The Forward-Backward Asymmetry of $e^+e^- \to b\bar{b}$ and $e^+e^- \to c\bar{c}$ Using Leptons in Hadronic Z^0 Decays*, CERN-PPE/93-78, submitted to Z. Phys. C.

Figure captions

Figure 1 Momentum and transverse momentum distributions of the electron and muon candidates in the data (points) and Monte Carlo (histogram). The contributions from the 5 components of the lepton candidate samples described in the text are indicated. The sum of the Monte Carlo components was normalized to the observed number of leptons in the data. The distributions contain only tracks passing all lepton selection and lepton identification criteria.

Figure 2 Distribution of the impact parameters before the detector simulation divided by the generated b hadron lifetime times the speed of light for electrons from b decays. Some entries are negative due to the signing procedure described in the text. The curve is the result of the fit using a sum of exponentials.

Figure 3 Distributions of the impact parameter divided by its associated error for electron resolution function tracks in (a) OPAL data and (b) Monte Carlo data. Figure (c) shows the corresponding distribution for Monte Carlo electrons after removing the lifetime content of the impact parameter. Similar distributions are obtained using the muon selection criteria. The curves are the result of a maximum likelihood fit using the function described in the text. Only negative entries are fitted in (a) and (b); the function is extrapolated into the positive region. The entire range is fitted in (c). The widths of the central Gaussians have been constrained to unity. The parametrized σ that results from this procedure is described in the text.

Figure 4 Distributions of the impact parameters for electron and muon candidates in the data. The curves are the result of the maximum likelihood fit for τ_b described in the text. The shaded area shows the contribution from all sources other than leptons produced in the semileptonic decay of b hadrons and in cascade decays.

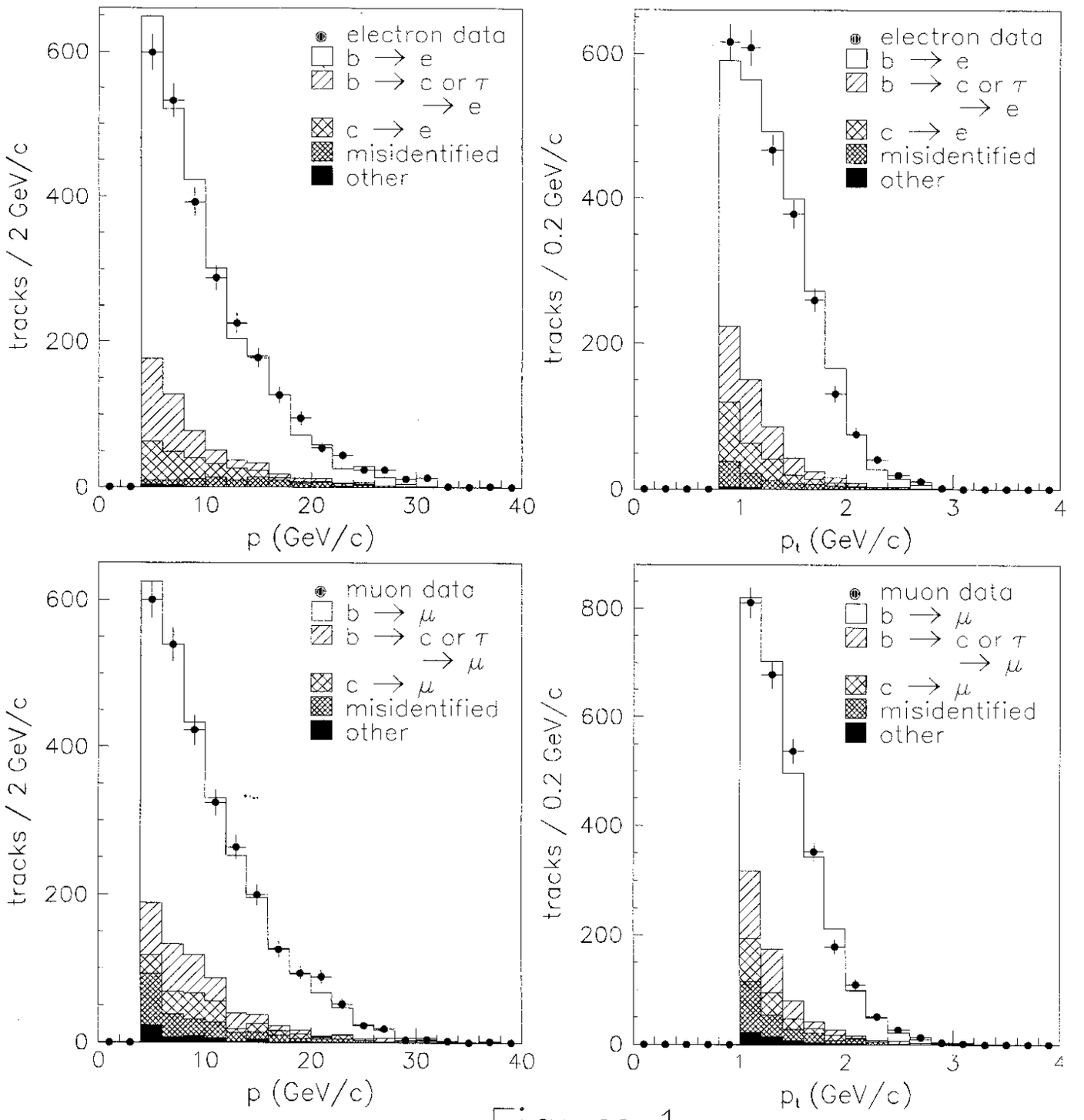
electron data
b → e
b → c or τ → e
c → e
misidentified
other
tracks / 2 GeV/c
p (GeV/c)
tracks / 0.2 GeV/c
p_t (GeV/c)
muon data
b → μ
b → c or τ → μ
c → μ
misidentified
other

Figure 1

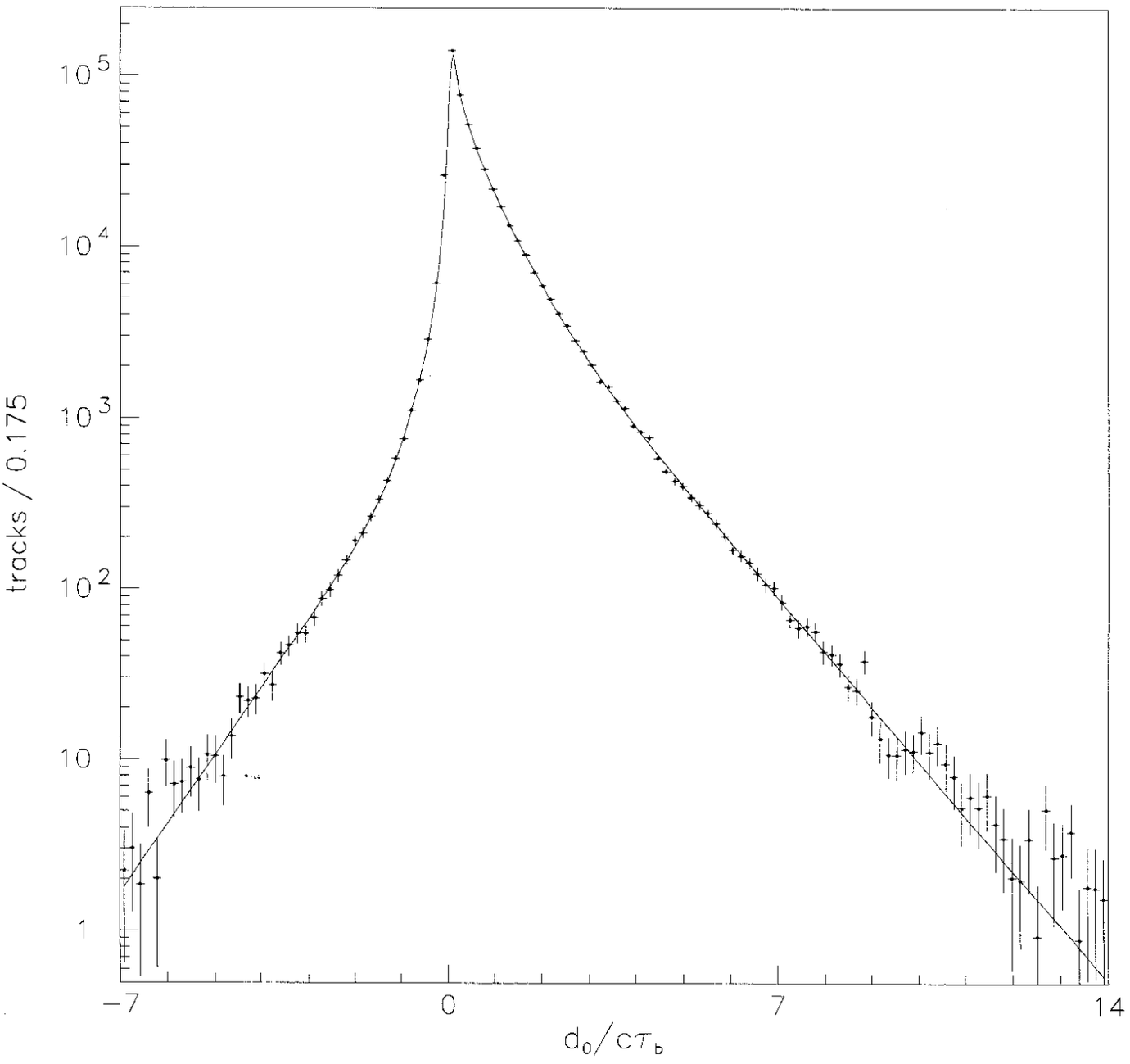

Figure 2

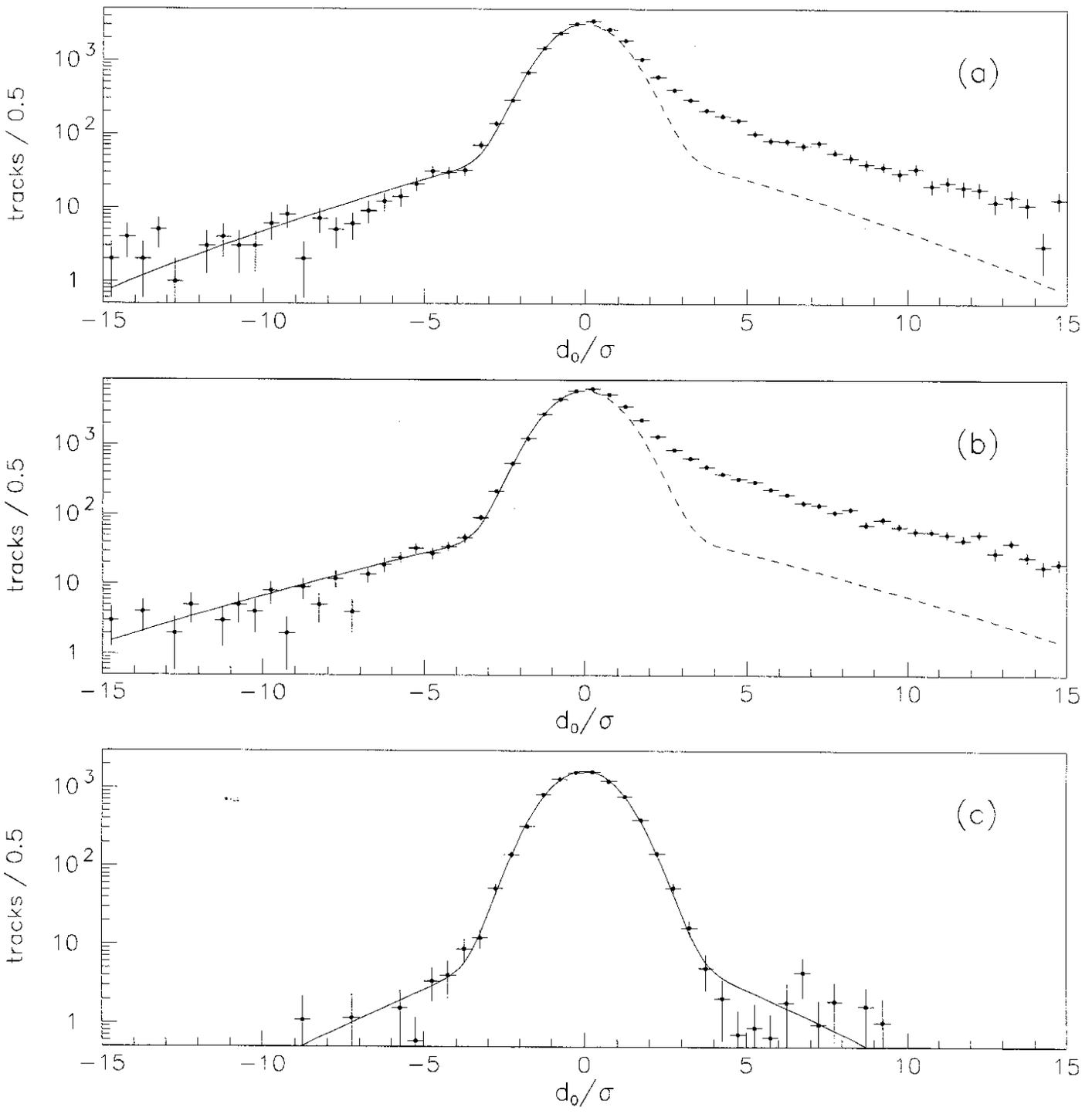
tracks / 0.5
10^3
10^2
10
1
(a)
−15
−10
−5
0
5
10
15
d_0/σ
tracks / 0.5
10^3
10^2
10
1
(b)
−15
−10
−5
0
5
10
15
d_0/σ
tracks / 0.5
10^3
10^2
10
1
(c)
−15
−10
−5
0
5
10
15
d_0/σ

Figure 3

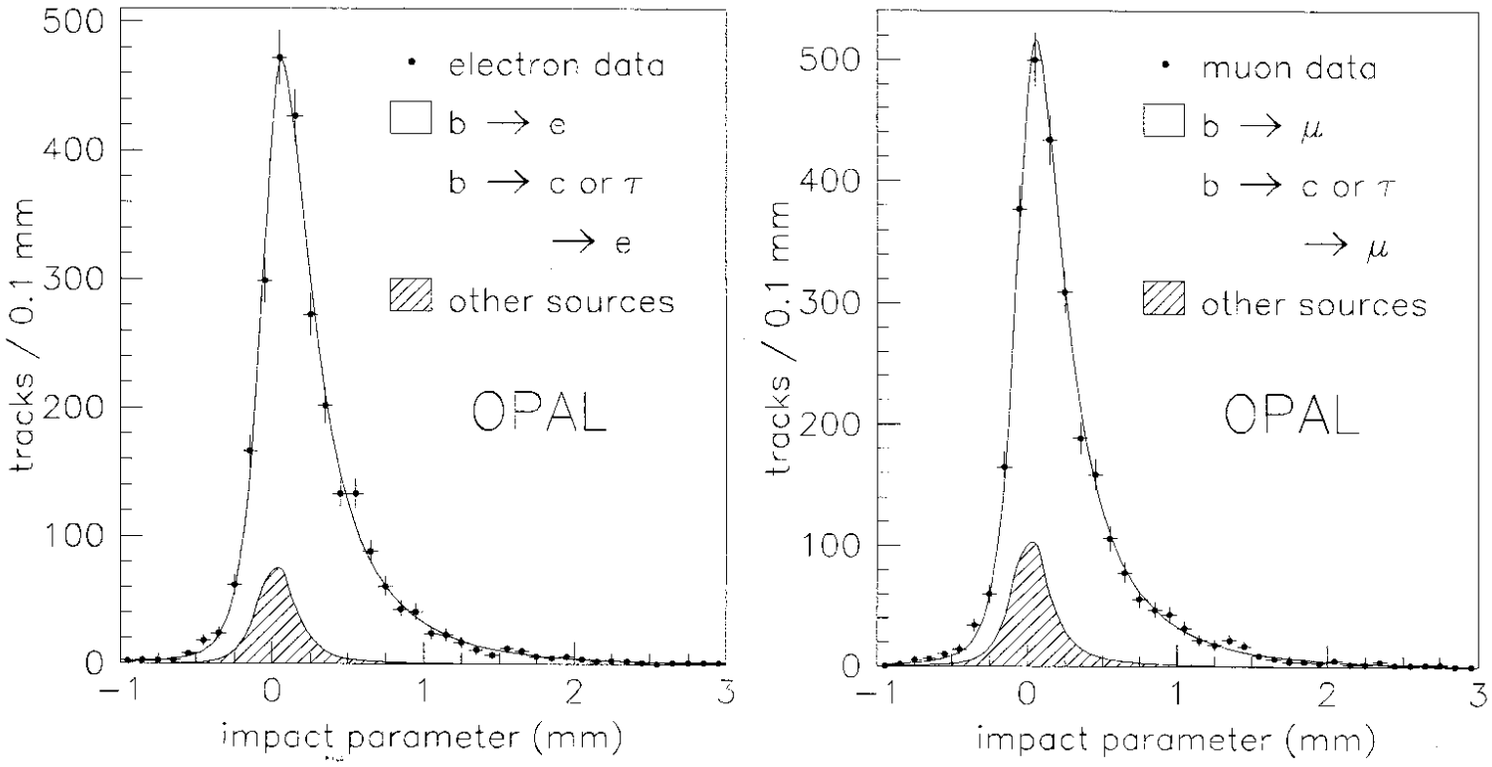
500
400
300
200
100
0
tracks / 0.1 mm
−1
0
1
2
3
impact parameter (mm)
• electron data
b → e
b → c or τ
→ e
other sources
OPAL
• muon data
b → μ
b → c or τ
→ μ
other sources
OPAL

Figure 4